DETECTION OF RADIO EMISSION FROM PULSARS

A pulsar observation primer

DIPANKAR BHATTACHARYA
Raman Research Institute
Bangalore 560 080, INDIA

1. Introduction

This lecture is intended to be a tutorial of the basic concepts and methods involved in the observation of Radio Pulsars. Pulsars, in general, are faint radio sources, and are consequently difficult to detect. In addition, the periodic signals from them suffer degradation due to propagation through the interstellar medium. As a result, special techniques are usually necessary to detect radio emission from pulsars, especially in pulsar surveys where new pulsars of unknown periods and unknown degree of line-of-sight dispersion are being searched for.

This presentation will discuss radio receiver basics (section 2), signal-to-noise issues (section 3), interstellar propagation effects on pulsar signals (section 4), dispersion removal techniques and their limitations (section 5) and pulsar survey procedure (section 6). A more detailed treatment of some of the topics discussed here can be found in Hankins and Rickett (1975).

2. Radio Receiver Basics

The schematic outline of a typical superheterodyne radio receiver is shown in figure 1. It consists of a reflector, typically a large dish antenna, which concentrates the received radiation at its focus, where a feed horn is placed. Inside the horn oscillating voltages are induced on sensors (usually two orthogonal dipoles for two linear polarizations) which are amplified by a low-noise amplifier (LNA) and sent down to the following electronics via cables. The feed horn + LNA assembly is tuned to a specific centre frequency $\nu_{\rm RF}$, with its response dropping off on either side of $\nu_{\rm RF}$. Modern installations, however, usually have a fairly wide usable bandwidth at this stage – a good fraction of the centre frequency. The final bandwidth used in the receiver is

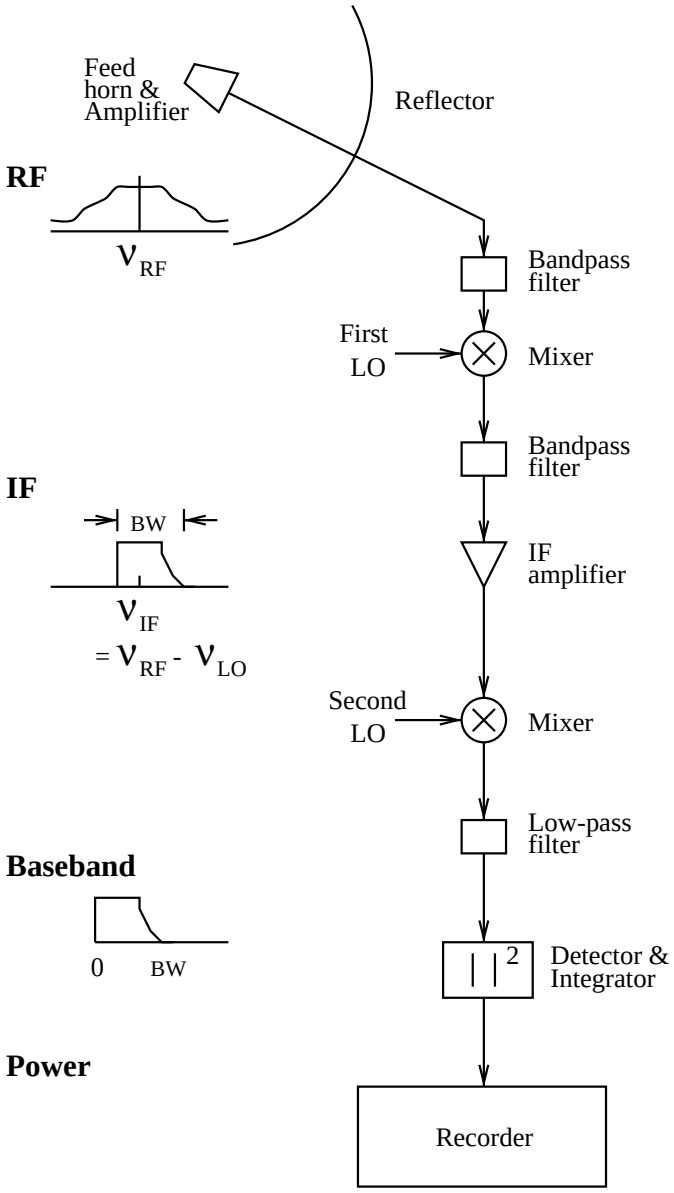

Figure 1. Schematic diagram of a Radio Telescope Receiver system.

usually decided by a set of bandpass filters the signal passes through after this stage in the rest of the electronics.

The RF signal then undergoes *mixing*, a name applied to beating the incoming signal with a stable monochromatic (i.e. of negligible bandwidth)

signal of frequency $\nu_{\rm LO}$ derived from a local oscillator (LO) at the observatory. The beating process generates signal at frequencies that are the sum and the difference of the incoming (RF) frequencies and $\nu_{\rm LO}$. A bandpass filter following the mixer passes the difference band, known as intermediate frequency (IF) for further processing. The centre frequency of the signal band has now been moved to $\nu_{\rm IF} = \nu_{\rm RF} - \nu_{\rm LO}$. The bandwidth BW of this signal, usually significantly smaller than that at RF, is set by the bandpass filters used.

A point to note here is that since the intermediate frequency is just the difference between $\nu_{\rm RF}$ and $\nu_{\rm LO}$, $\nu_{\rm RF} = \nu_{\rm LO} + \nu_{\rm IF}$ and $\nu_{\rm RF} = \nu_{\rm LO} - \nu_{\rm IF}$ result in the same intermediate frequency $\nu_{\rm IF}$, causing an ambiguity at this stage. The former band ($\nu_{\rm RF} > \nu_{\rm LO}$) is called the Upper Side Band (USB) and the latter ($\nu_{\rm RF} < \nu_{\rm LO}$) the Lower Side Band (LSB). To circumvent this ambiguity, one either uses a sideband separation technique by using two local oscillators at quadrature, or eliminates one of the sidebands before the mixer using a suitable bandpass filter. In what follows, I shall, for the sake of simplicity, assume that always the upper sideband alone is chosen after mixing, ensuring that the order of frequencies before and after mixing is the same (i.e., increasing $\nu_{\rm IF}$ corresponds to increasing $\nu_{\rm RF}$ after the first mixing stage).

The IF band is then passed through an amplifier, following which one of several things could be done: it could be detected and recorded right after this, or could be passed through a filter bank to split the signal into many narrow frequency channels, each of which can be separately detected and recorded (this makes up an analog multi-channel spectral receiver), or, as in several modern installations, be brought down to Baseband by mixing with a local oscillator and producing a band going from frequency 0 Hz to BW (see figure 1) before detection. The baseband could also be digitally sampled at Nyquist rate (sampling interval = $1/(2 \cdot \mathrm{BW})$) using analog-to-digital converters, passed through a digital spectrometer or a coherent dedispersing hardware (see section 5) before detection and recording.

The process of detection usually comprises of passing the signal through a device with square-law response (output proportional to square of the input), which converts the signal proportional to voltage (at the input) into a signal proportional to the total power in the band (at the output). The detected power is usually integrated (averaged) for a certain length of time before recording.

3. Signal-to-Noise issues

In figure 2 is shown a typical example of the progression of the signal from voltage (pre-detection) to power (post-detection) and the final output after

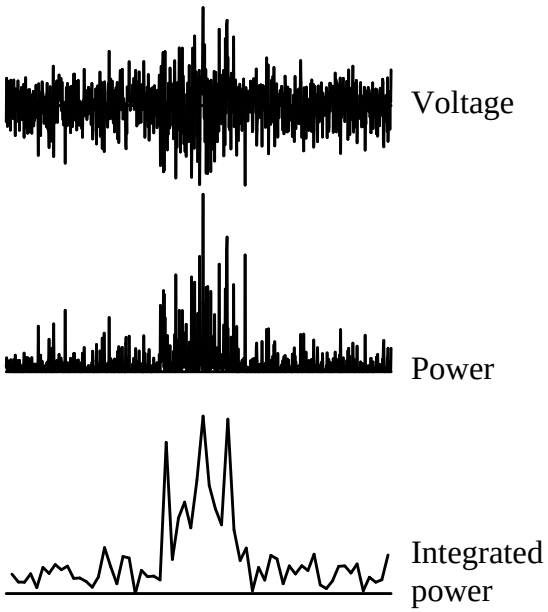

Figure 2. Process of detection and integration. The top panel shows the pre-detection voltage, middle panel the power immediately after square-law detection, and the bottom panel shows the power output after integration (boxcar averaging) of 16 consecutive samples. The horizontal axis is time, and the vertical axes are in arbitrary units.

integration (averaging). As indicated in the figure, the voltage fluctuations are two-sided, with zero mean. On detection (squaring), the resultant quantity, power, is positive definite. The mean of this positive definite signal is proportional to the total power in the band. Before integration, the rms (root mean square) of this time series is nearly equal to the mean itself. At the centre of the displayed time series exists some additional power due to a source, while the rest of it has just receiver and background noise. On passing through an integrator, N consecutive samples of the power time series is averaged. This leaves the mean of the time series unaltered, but reduces the rms by a factor $N^{1/2}$. As a result, the signal-to-noise ratio of a source, defined as

$$\mathrm{SNR} = \frac{\text{on-source mean} - \text{off-source mean}}{\text{off-source rms}}$$

is improved by a factor $N^{1/2}$, as seen in the bottom panel of figure 2.

As should also be clear from this figure, the signal from a source is of essentially the same nature as background noise, so the only thing that happens on-source is a rise in the average power over the band. Whether

this rise in power is detectable or not depends on the signal-to-noise ratio (SNR) defined above being higher than a reasonable threshold.

For a signal with bandwidth BW, independent samples are available at a time interval of $\Delta t = 1/\mathrm{BW}$. An 'integration time' τ therefore yields $\mathrm{BW} \times \tau$ independent samples. If two orthogonal polarisations are also averaged after detection, the relevant number of independent samples rises to $N = 2.\mathrm{BW}.\tau$.

In a radio receiver, the 'noise' is contributed by the local electronics – amplifiers, mixers, detectors and other components. This is called the 'receiver noise'. The telescope, while observing a radio source of interest, also picks up signal from other sources, and diffuse background in the beam. This unnecessary (but unavoidable) signal from the sky adds to the background 'noise' in the system. This component is referred to as the 'sky noise'. The power in a radio receiver is usually expressed as a temperature – a noise temperature T being equal to the amount of noise power picked up by a dipole (in the band of interest) when immersed in a black-body bath of temperature T. The noise contributed by receiver elements is thus denoted as T_{rec} and the sky noise as T_{sky}. The net background noise in the system is thus $T_{\mathrm{rec}} + T_{\mathrm{sky}}$. The 'signal' from a source, as noted above, is also noise-like. The presence of the source is reflected in an enhancement of the noise power by T_{A}, called the 'Antenna temperature'. The antenna temperature is, of course, proportional to the source flux, and is related to it by

$$\begin{aligned} T_{\mathrm{A}} &= G.S \\ G &= \frac{A_{\mathrm{e}}}{2k_{\mathrm{B}}} \end{aligned}$$

where S is the flux per unit frequency interval from the source, A_{e} is the effective collecting area of the telescope and k_{B} is the Boltzmann constant. The value of G works out to be about 1 K/Jy for an A_{e} of 2700 m^2. Jansky (Jy) is the standard unit of spectral flux in radio astronomy, equal to 10^{-26} W m^{-2} Hz^{-1}.

In terms of the temperatures, then, we can express the signal-to-noise ratio of the source in the following way. The off-source mean is $(T_{\mathrm{rec}} + T_{\mathrm{sky}})$, and therefore the off-source rms after integration is $(T_{\mathrm{rec}} + T_{\mathrm{sky}})/\sqrt{N_{\mathrm{pol}}.\mathrm{BW}.\tau}$, where N_{pol} is the number (1 or 2) of orthogonal polarisations averaged. Since the excess noise temperature on-source is T_{A}, the signal-to-noise ratio is

$$\begin{aligned} \mathrm{SNR} &= \frac{T_{\mathrm{A}}}{T_{\mathrm{rec}} + T_{\mathrm{sky}}} \sqrt{N_{\mathrm{pol}}.\mathrm{BW}.\tau} \\ &= G.S \frac{\sqrt{N_{\mathrm{pol}}.\mathrm{BW}.\tau}}{T_{\mathrm{rec}} + T_{\mathrm{sky}}} \end{aligned} \qquad (1)$$

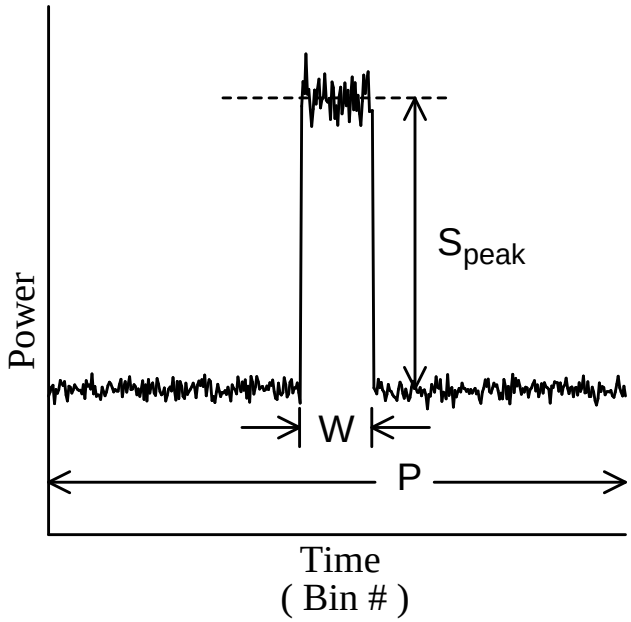

Figure 3. An idealised folded pulse profile. P is the pulse period, W is the pulse width and $S_{\rm peak}$ is the peak flux of the pulsar.

If β is the minimum SNR for a source to be considered detected, then the minimum detectable flux in this observation would be

$$S_{\rm min} = \frac{\beta}{G} \frac{T_{\rm rec} + T_{\rm sky}}{\sqrt{N_{\rm pol}.{\rm BW}.\tau}}$$

In case of a pulsar, the data obtained from the receiver can be folded at the pulse period to enhance the SNR of the pulse. As shown in figure 3, this results in a folded profile with a certain number of chosen bins across the period P. If the number of bins is $N_{\rm b}$, then the effective integration time in this case is the integration time per bin, which is equal to $\tau/N_{\rm b}$, where τ now stands for the total duration of observation using which the folded profile has been constructed. The peak of the folded profile corresponds to a flux $S_{\rm peak}$, which lasts for a duration W (pulse width) in every period (see figure 3). The pulse width W here includes all broadening effects due to propagation through the interstellar medium (see section 4) as well as the instrumental response. The minimum detectable $S_{\rm peak}$ can then be written as

$$S_{\rm peak,min} = \frac{\beta}{G} \frac{T_{\rm rec} + T_{\rm sky}}{\sqrt{N_{\rm pol}.{\rm BW}.\tau}} \sqrt{N_{\rm b}} \qquad (2)$$

However, it is customary to quote the detection limit in terms of the *average* flux of the pulsar $S_{\rm av} = (W/P) \times S_{\rm peak}$:

$$S_{\rm av,min} = \frac{\beta}{G} \frac{T_{\rm rec} + T_{\rm sky}}{\sqrt{N_{\rm pol}.{\rm BW}.\tau}} \sqrt{N_{\rm b}} \frac{W}{P} \tag{3}$$

The best SNR is, of course, obtained if all the flux of the pulsar is collected into one bin, i.e. having bins of width equal to W. This would result in $N_{\rm b} = (P/W)$. However, this is possible only as long as $W \ll P$. In the other extreme, $W \geq P/2$, one has to choose the bin width to define the off-pulse region properly, so the bin width should be $(P - W)$. $N_{\rm b}$ in this case would be $P/(P - W)$. Inserting these in eq. (3) one ends up with

$$S_{\rm av,min} = \frac{\beta}{G} \frac{T_{\rm rec} + T_{\rm sky}}{\sqrt{N_{\rm pol}.{\rm BW}.\tau}} \sqrt{\frac{W}{P}} \quad (W \ll P) \tag{4}$$

$$S_{\rm av,min} = \frac{\beta}{G} \frac{T_{\rm rec} + T_{\rm sky}}{\sqrt{N_{\rm pol}.{\rm BW}.\tau}} \frac{W}{\sqrt{P(P - W)}} \quad (W \geq P/2) \tag{5}$$

The following expression, widely used in the literature, is an interpolation between the two limits, approaching both eq. (4) and eq. (5) asymptotically:

$$S_{\rm min} = \frac{\beta}{G} \frac{T_{\rm rec} + T_{\rm sky}}{\sqrt{N_{\rm pol}.{\rm BW}.\tau}} \sqrt{\frac{W}{(P - W)}} \tag{6}$$

This relation can be arrived at by assuming that irrespective of pulse width the entire on-pulse region is averaged into one bin of width W, and the entire off-pulse region into another bin of width $(P - W)$, following which the signal-to-noise ratio is defined as the difference of the two means divided by the rms of the *difference* (see Vivekanand et al 1982).

4. Effects of propagation through interstellar plasma on pulsar signal

Let us now discuss the relation between the signal actually emitted from a source and that recorded by a radio receiver. The signal travels a long distance through the interstellar space to reach us. The interstellar space contains a large-scale distribution of ionised gas (plasma) which modifies the characteristics of the signal passing through it. To start with, let us assume that the plasma is homogeneous. The signal $S(t)$ emitted by the source can be written in terms of its frequency components as:

$$S(t) = \int_{-\infty}^{\infty} S(\nu) {\rm e}^{-i2\pi\nu t}\, d\nu$$

Signal at a frequency component ν, starting at source as

$$S(\nu)\mathrm{e}^{-i2\pi\nu t},$$

and traversing the distance L between the source and the observatory, arrives at the observatory as

$$S(\nu)\mathrm{e}^{-i(2\pi\nu t - kL)}.$$

where ν and k are related by the dispersion relation

$$\nu^2 = \nu_\mathrm{p}^2 + \frac{c^2}{4\pi^2}k^2 \tag{7}$$

$$\nu_\mathrm{p}^2 = \frac{n_\mathrm{e}e^2}{\pi m_\mathrm{e}} \tag{8}$$

Here ν_p is the plasma frequency of the medium, n_e is the electron density in the plasma, e and m_e are the charge and mass of an electron respectively. c is the speed of light in vacuum.

Under typical interstellar conditions the plasma frequency ν_p is of order 2 KHz, much smaller than the typical frequency at which radio observations are made (hundreds to thousands of MHz). From eq. (7) the relation between k and ν then becomes

$$\begin{aligned} k &= \frac{2\pi\nu}{c}\left(1 - \frac{\nu_\mathrm{p}^2}{\nu^2}\right)^{1/2} \\ &= \frac{2\pi\nu}{c}\left(1 - \frac{\nu_\mathrm{p}^2}{2\nu^2}\right) \quad (\nu \gg \nu_\mathrm{p}) \end{aligned} \tag{9}$$

up to the leading order in ν_p^2/ν^2.

The signal at frequency component ν arriving at the observatory can now be written using eq. (9) as

$$S(\nu)\mathrm{e}^{-i2\pi\nu t} \cdot \mathrm{e}^{i\phi_\mathrm{p}}$$

with

$$\phi_\mathrm{p} = 2\pi\nu\frac{L}{c}\left(1 - \frac{\nu_\mathrm{p}^2}{2\nu^2}\right) \tag{10}$$

being the phase acquired by propagation.

The frequency ν in the observed signal runs from ν_l to ν_u, the radio frequencies corresponding to the lower and the upper edge of the band. The bandwidth BW$= \nu_\mathrm{u} - \nu_\mathrm{l}$. Eventual conversion of this frequency band

to baseband is equivalent to multiplying this signal with a local oscillator at the lower edge of the band, ν_l:

$$\begin{aligned} & S(\nu)\mathrm{e}^{-i2\pi\nu t}\cdot\mathrm{e}^{i\phi_\mathrm{p}} \otimes \mathrm{e}^{i2\pi\nu_\mathrm{l}t} \\ \Rightarrow\quad & S(\nu)\mathrm{e}^{-i2\pi(\nu-\nu_\mathrm{l})t}\cdot\mathrm{e}^{i\phi_\mathrm{p}} \\ & = S(\nu)\mathrm{e}^{-i2\pi\nu_\mathrm{b}t}\cdot\mathrm{e}^{i\phi_\mathrm{p}} \end{aligned}$$

where $\nu_\mathrm{b} = \nu - \nu_\mathrm{l}$ is the corresponding baseband frequency, lying in the range 0 Hz to BW. Because of amplifications on the way, the baseband output (prior to detection) is a scaled version of the above:

$$A(\nu_\mathrm{b})\mathrm{e}^{-i2\pi\nu_\mathrm{b}t}\cdot\mathrm{e}^{i\phi_\mathrm{p}}$$

with $A(\nu_\mathrm{b}) \propto S(\nu)$. The pre-detection baseband voltage is a combination of such amplitudes over the entire band BW

$$V(t) = \int_0^{\mathrm{BW}} A(\nu_\mathrm{b})\mathrm{e}^{-i2\pi\nu_\mathrm{b}t}\cdot\mathrm{e}^{i\phi_\mathrm{p}}\,d\nu_\mathrm{b}$$

When this voltage is passed through a square-law detector, the quantity $P(t) = |V(t)|^2$ is created, which is proportional to the net power over the entire band, but the identity of the individual frequencies is lost in doing so.

4.1. DISPERSION

The effect of the propagation through a homogeneous medium is contained in the phase factor ϕ_p above. As can be seen, the phase factor is frequency dependent, caused by a frequency dependence of the phase velocity. This results in the arrival time of a pulse being frequency dependent, even though at the source the pulse is emitted simultaneously over a wide band. The lower the radio frequency, the later the pulse arrives. This *dispersion* within the observed bandwidth (BW) causes the pulse to be broadened once the signal of the entire band is put together (e.g. by detection) without special measures being employed to 'dedisperse' the signal. Methods for dedispersion will be discussed in section 5. At this point, let us estimate the amount of dispersion delay suffered by the band. To do so, we note that the propagation delay τ_ν at a radio frequency ν is given by

$$\tau_\nu \;=\; \frac{1}{2\pi}\frac{d\phi_\mathrm{p}}{d\nu} \;=\; \frac{L}{c}\left(1+\frac{\nu_\mathrm{p}^2}{2\nu^2}\right)$$

The *dispersion delay* at a frequency ν is then

$$\mathcal{D}_\nu \;=\; \tau_\nu - \tau_\infty \;=\; \frac{L}{c}\cdot\frac{\nu_\mathrm{p}^2}{2\nu^2} \;=\; \frac{e^2}{2\pi m_\mathrm{e}c}\cdot(n_\mathrm{e}L)\cdot\frac{1}{\nu^2} \qquad (11)$$

$$= \quad 4150 \text{ s } \left(\frac{\text{DM}}{\text{cm}^{-3}\text{pc}}\right)\left(\frac{\nu}{1 \text{ MHz}}\right)^{-2} \tag{12}$$

where DM is the *Dispersion Measure* defined as

$$\text{DM} = \int_0^L n_\text{e}\, dl \tag{13}$$

To illustrate the effect of dispersion, figure 4 displays the pulse of the pulsar B 1642 − 03 recorded in a number of adjacent frequency bands, each 250 KHz wide, at the Ooty Radio Telescope. The delay in the arrival time between channels is clearly visible.

4.2. SCATTERING AND SCINTILLATION

So far we have discussed the effect of signal propagation through a homogeneous medium. In reality, the interstellar plasma is inhomogeneous, containing concentrations of electron density with a wide distribution of sizes. This causes irregular distortion of the propagating waveform, resulting in scattering of the signal. A relative motion between the source, observer and the scattering medium causes the phenomenon of interstellar scintillation. The study of interstellar scintillation and scattering is a vast field in itself, the interested reader is referred to detailed reviews by Rickett (1977) and Rickett (1990) as well as the references therein. Here we give a short, qualitative introduction. The process of scattering is schematically outlined in figure 5. For a simple description, let us assume that the size distribution of irregularities is a Gaussian with a typical scale of a. Panel (a) shows the corrugation of the wavefront (highly exaggerated) after passing through a layer of electron density irregularities of scale size a. A change in electron density corresponds to a change in refractive index μ, and this contributes a phase deviation

$$\delta\phi = 2\pi\nu\frac{a}{c}\Delta\mu = 2\frac{a}{c}\cdot\frac{\Delta n_\text{e} e^2}{m_\text{e}\nu}$$

After propagating through a distance L, about $\sqrt{L/a}$ such irregularities are encountered, resulting in an rms phase deviation

$$\Delta\phi \sim \left(\frac{L}{a}\right)^{1/2}\delta\phi \sim (La)^{1/2}\frac{e^2}{m_\text{e}c}\Delta n_\text{e}\cdot\frac{1}{\nu}$$

The phase difference $\Delta\phi$ over the length scale a bends the wavefront by an amount θ_sc, which can be written as (see panel (b) of fig 5)

$$\theta_\text{sc} \approx \frac{\Delta z}{a} = \frac{c}{2\pi a}\cdot\Delta\phi\cdot\frac{1}{\nu}$$

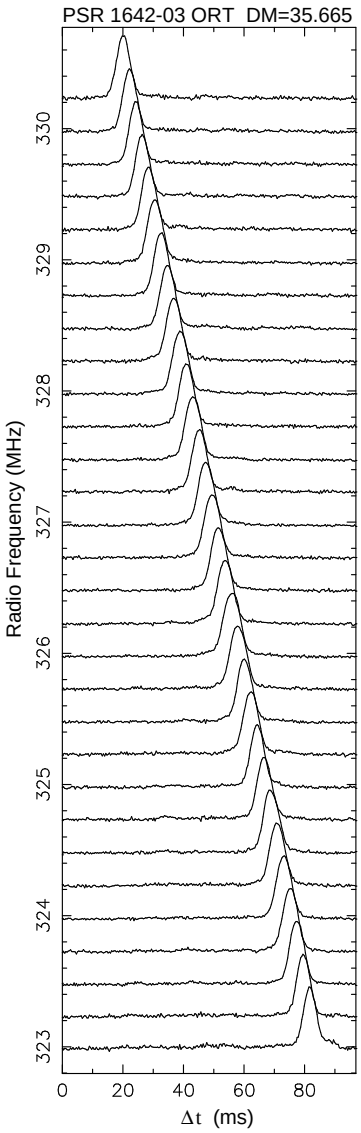

Figure 4. Pulse profile of PSR 1642−03 recorded using the Ooty Radio Telescope (ORT) at adjacent frequency channels separated by 250 KHz. Each profile shown is produced by folding a 9-minute long data stream at the pulse period of 387.65 ms. No dispersion correction has been applied. Only a portion of the full period is shown. The dispersion delay in pulse arrival time between the channels is clearly visible. Over the 8 MHz band displayed, the signal suffers a delay of more than 60 ms. The delay gradient appears to be linear at first sight because the bandwidth in use is rather small. However placing a ruler over the pulse peaks would clearly reveal the non-linearity. The Dispersion Measure of this pulsar is 35.665 pc cm^{-3}.

Substituting for $\Delta\phi$ one obtains

$$\theta_{\rm sc} \approx \frac{1}{2\pi}\left(\frac{L}{a}\right)^{1/2} \cdot \frac{e^2 \Delta n_{\rm e}}{m_{\rm e}} \cdot \frac{1}{\nu^2} \qquad (14)$$

A Gaussian distribution of scattering angles with scale $\theta_{\rm sc}$ is generated in the process. Panel (c) of figure 5 shows the relation between the scattering angle $\theta_{\rm sc}$ and the observed half-angular width of the scattering disc: $\theta_0 = \theta_{\rm sc}/2$. The entire scattering process has been approximated to take place in a screen placed halfway between the source and the observer. This is a good first approximation if the distribution of scattering material is uniform along the line-of-sight. The intensity distribution in the scattered image of a point source is now

$$I(\theta)\, d\theta \sim {\rm e}^{-\theta^2/\theta_0^2} \cdot 2\pi\theta \frac{d\theta}{\pi\theta_0^2}$$

What the scattering process does to the pulsar signal is that the observer receives the signal not only along the direct route from the source to the observer, but also along the scattered routes. The scattered routes are of course longer and therefore the signal arriving by them are delayed with respect to the direct route. As a result, a sharp signal like a pulse gets broadened. The larger the scattering disc, the broader the pulse becomes. A signal arriving from an angle θ away from the direct path (of length L) traverses an extra distance $L\theta^2/2$, and hence arrives with a delay $\Delta t(\theta) = L\theta^2/(2c)$. Given the intensity distribution $I(\theta)$ above, one would then expect the delayed arrivals to follow an intensity law

$$\begin{aligned} I(\Delta t) &= I(\theta)/\left(\frac{d\Delta t}{d\theta}\right) \propto {\rm e}^{-\Delta t/\tau_{\rm scat}} \\ \text{where } \tau_{\rm scat} &= \frac{L}{2c}\theta_0^2 \approx \frac{1}{2ac}\left(\frac{e^2\Delta n_{\rm e}}{4\pi m_{\rm e}}\right)^2 \frac{L^2}{\nu^4} \end{aligned}$$

Panel (d) of figure 5 shows the observed profile for an impulse function emission. The signal arriving by the direct route arrives first, creating the sharp rise, and then the signals arriving by delayed routes create the exponential tail. Scattered pulse profiles of this shape are readily observed, particularly at long wavelengths where this effect is very strong (see ν^{-4} dependence above). An example is shown in figure 6.

The true distribution of irregularities in the interstellar medium is, however, not of one characteristic length a, but is closer to a power law. In wave number space the irregularity spectrum is usually written as

$$P(q) = C_n^2 q^{-\beta} \quad \text{where } q = \text{wavenumber} = \frac{2\pi}{a}$$

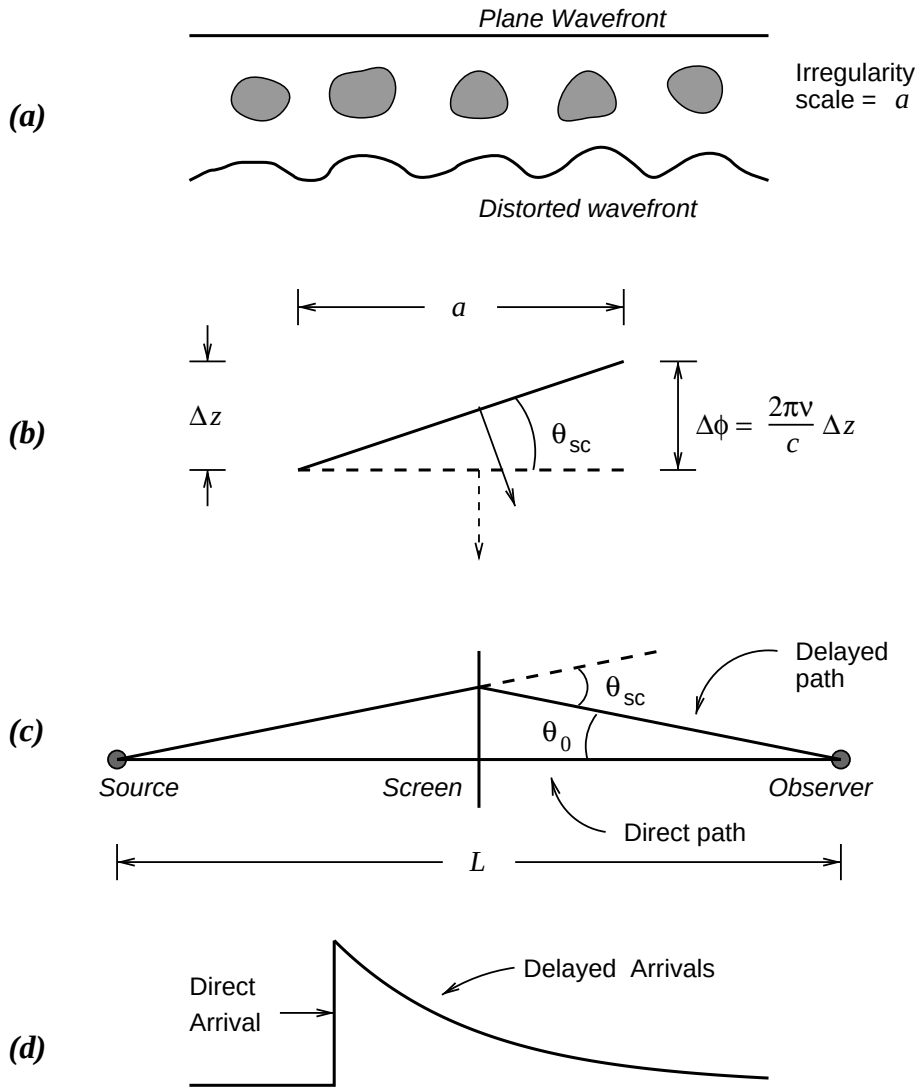

Figure 5. Scattering of pulsar signal due to propagation through irregularities in the electron density distribution in the interstellar medium. Panel (*a*) shows the distortion of a plane wavefront on passing through electron density irregularities. Panel (*b*) displays the relation between the phase gradient and scattering angle. Panel (*c*) shows the multipath propagation of the signal due to scattering, and panel (*d*) shows the truncated exponential pulse profile resulting from delays in multipath propagation (in this figure the intrinsic pulse width is assumed to be zero).

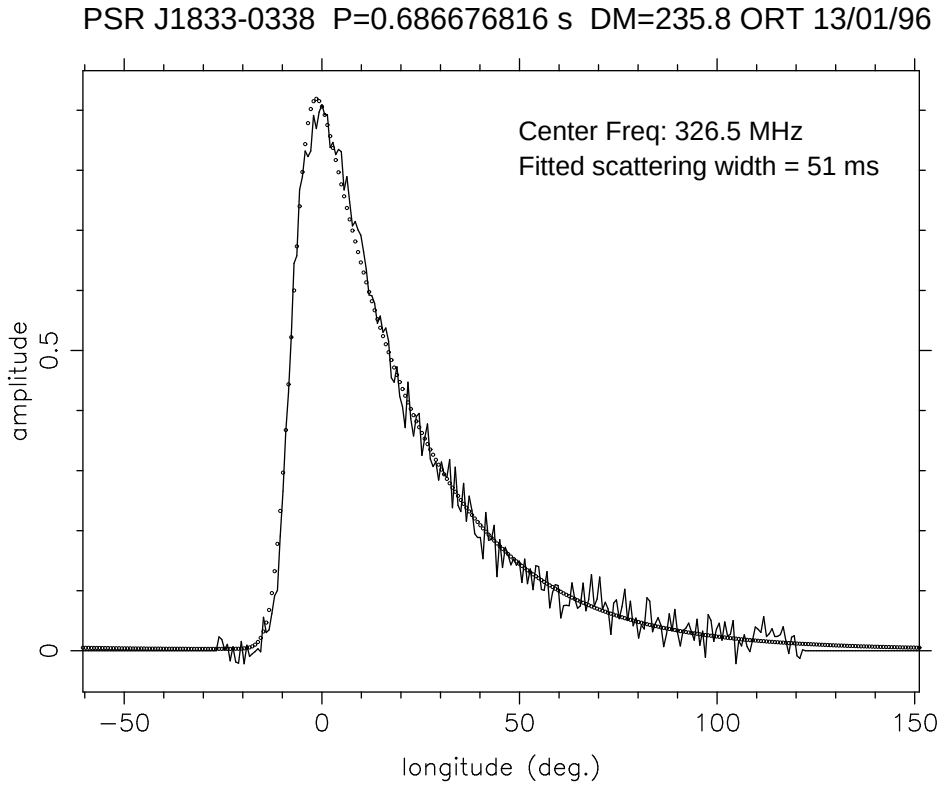

Figure 6. Pulse profile of PSR J1833-0338 observed with the Ooty Radio Telescope. The exponential scattering tail dominates the pulse width. The open circles show a fit to the profile, with an assumed scattering width of 51 ms. From Ramachandran et al (1997).

This spectrum modifies the above results somewhat, resulting in the following scaling laws with frequency:

$$\begin{aligned} \theta_0 &\propto \nu^{-\beta/(\beta-2)} \\ \tau_{\rm scat} &\propto \nu^{-2\beta/(\beta-2)} \end{aligned}$$

For a pure Kolmogorov spectrum arising out of turbulence, $\beta = 11/3$, which yields $\tau_{\rm scat} \propto \nu^{-4.4}$. This appears to fit the observed scattering widths of pulsars very well.

The phenomenon of multipath propagation has another, related, effect. At a given time of observation the received signal corresponds not to a single instant of emission but to a range of emission times of duration $\sim \tau_{\rm scat}$. This corresponds to a range of phases in the received signal, of width $\sim 2\pi\nu\tau_{\rm scat}$, where ν is the observing frequency. Interference of signals with this phase range produces a scintle pattern in the observing plane, with patches of

enhanced and reduced intensity. If the line of sight from the observer to the source moves with respect to the scattering medium, which does happen in the case of a pulsar because of the proper motion of the pulsar as well as the motion of the earth in its orbit, then this scintle pattern moves with respect to the observer giving rise to a fluctuation of the observed intensity. This is known as Diffractive Interstellar Scintillation. Since for a given $\tau_{\rm scat}$ the phase range of received signal is frequency dependent, the scintle pattern also depends on frequency. By the time the phase range differs by more than ~ 1 radian, the scintillation pattern at the two frequencies are essentially independent. This defines the so-called *decorrelation bandwidth*, within which there is a non-vanishing correlation in the scintillation pattern. From the above condition, we find that the decorrelation bandwidth is given by

$$2\pi\Delta\nu\tau_{\rm scat} \simeq 1, \quad \text{i.e. } \Delta\nu \simeq \frac{1}{2\pi\tau_{\rm scat}}$$

At high (GHz) frequencies, where the scattering width is small, the decorrelation bandwidth is a good way of measuring $\tau_{\rm scat}$, and is often used for the purpose.

Observations indicate that there is a good degree of correlation between the scattering width (at any given frequency) and the dispersion measure of pulsars. This is not very surprising, as a larger dispersion measure in general means a longer path length of propagation through the interstellar medium, which would also, in general, mean that the signal encounters a larger number of electron density fluctuations (see Taylor and Cordes (1993) for a detailed discussion). An empirical fit between $\tau_{\rm scat}$ and DM made by Bhattacharya et al (1992) is expressed as a sum of two power laws:

$$\begin{aligned} \tau_{\rm scat}\,(400\ {\rm MHz}) \quad = \quad & 10^{-4.62\pm0.52+(1.14\pm0.53)\log {\rm DM}} \\ & +10^{-9.22\pm0.62+(4.46\pm0.33)\log {\rm DM}} \ {\rm ms} \end{aligned} \tag{15}$$

There is an additional component of interstellar scintillation, caused by irregularities of very large scale. Refractive index variations on these scales result in focussing and defocussing of the scintillation pattern in the observing plane. This is known as the Refractive Interstellar Scintillation and is responsible for long-term (months to years) variation of flux received from pulsars, particularly at metre wavelengths.

5. Dispersion Removal Techniques

5.1. INCOHERENT DEDISPERSION

As discussed in section 4, propagation through the interstellar medium causes dispersion of the pulsar signal, making the pulse arrive later at a

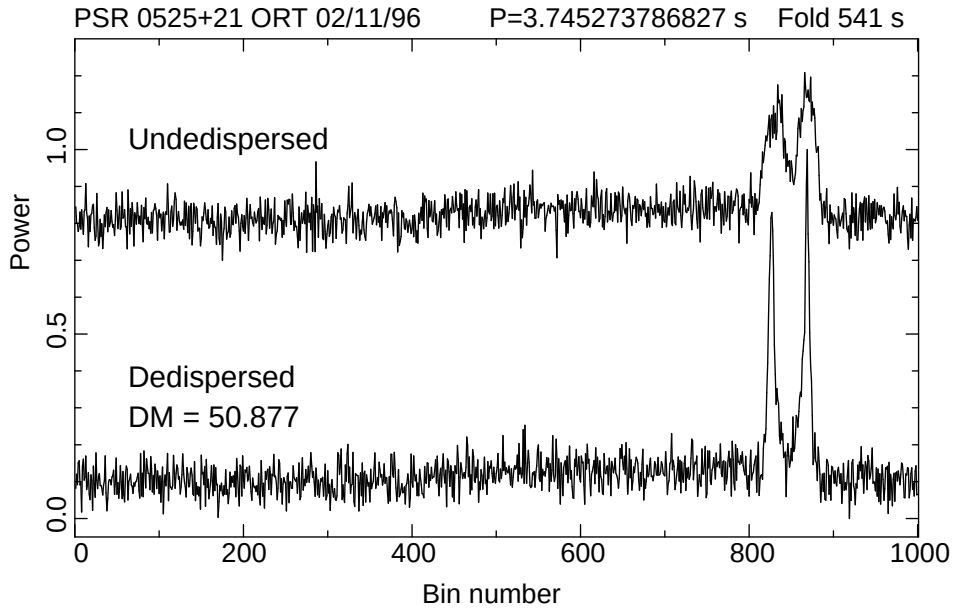

Figure 7. An example of incoherent dedispersion. PSR 0525+21 was observed using the Ooty Radio Telescope in 256 adjacent frequency channels, each 31.25 KHz wide, making up a total bandwidth of 8 MHz centred at 326.5 MHz. A data stretch of 541 seconds was folded to generate the displayed profile. The upper track shows the profile produced if no dispersion correction is applied between the frequency channels, and the lower panel shows the same data put together after dispersion delays corresponding to the known DM of 50.877 have been compensated for.

lower frequency. This results in broadening of the pulse and consequent loss of signal-to-noise ratio if the signal over the whole observing band is combined. One simple way of alleviating this problem is to split the full bandwidth into a number of narrow bands (as shown in figure 4), record the signal from each of these sub-bands in parallel, and after detection apply an appropriate delay to the output of each band so as to line up the pulses, compensating for the dispersion delay suffered in propagation. The signals from the sub-bands may now be combined to yield a dispersion-corrected pulse profile. If this is done to the time series shown in figure 4 the resulting pulse width would be only about 5 ms, whereas if the delay correction is not applied the pulse width after combination will become as large as $\sim$ 60 ms. This technique is known as *incoherent dedispersion*, since the signals are combined after detection. Figure 7 shows an example of the pulse narrowing and improvement in signal-to-noise ratio obtained employing this technique.

It is clear, however, that in the process of incoherent dedispersion the

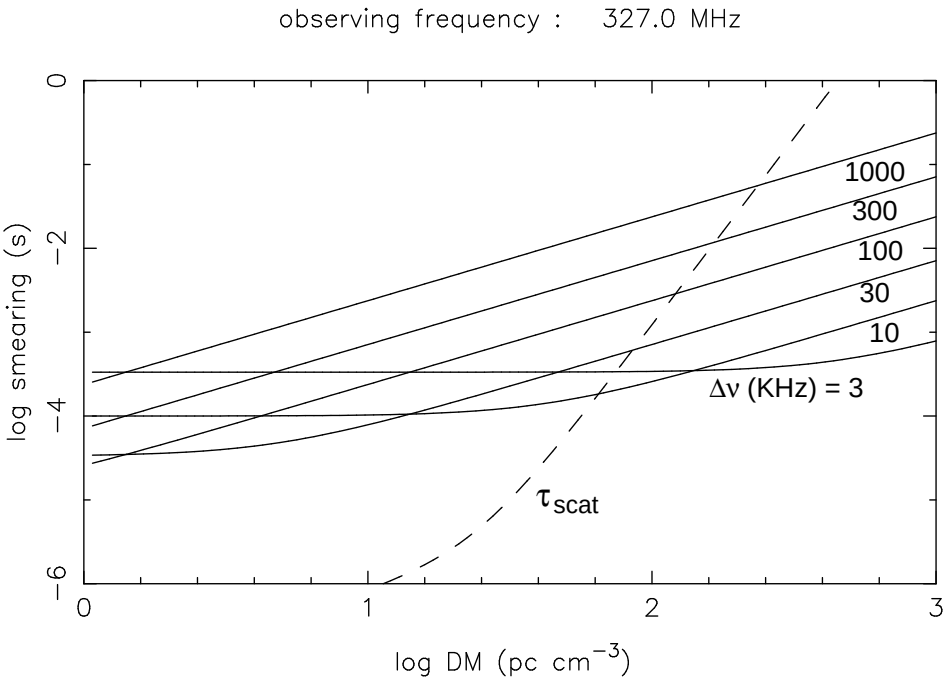

Figure 8. Effective time resolution on a pulse profile as a function of Dispersion Measure and channel bandwidth $\Delta\nu$ in incoherent dedispersion technique. At low dispersion, the inverse bandwidth response restricts the time resolution (the horizontal portions of the curves), and at higher DMs the dispersion delay dominates (the sloping portions). The inflection points of the curves correspond to the optimum channel bandwidth for the DM. A tangent to these inflection points gives the best achievable time resolution using incoherent dedispersion, as a function of DM. As can be seen, at an observing frequency of 327 MHz, for which the curves are displayed, it is not possible to achieve a time resolution better than ~ 30 μs even for very nearby pulsars with low DMs. The dashed line shows the limitation imposed by scatter broadening. $\tau_{\rm scat}$ is computed using eq. 15. After Deshpande (1989).

dispersion delay inside each of the sub-bands remains uncorrected. Therefore if the frequency sub-bands are not narrow enough, the dispersion delay may still dominate the pulse width, particularly at high dispersion measures and at low frequencies. This sets a limit to the time resolution one can achieve on the pulse profile. Of course, the degree to which dispersion delay can be corrected can be improved by making the frequency channels arbitrarily narrow, but one then comes up against another limit: a frequency channel of width $\Delta\nu$ will provide independent samples only at time intervals of $1/\Delta\nu$, so it is impossible to achieve a time resolution better than this. For a given observing frequency and DM this therefore suggests an optimum channel bandwidth, below which the sampling limit prevails and above which the dispersion smearing dominates. Figure 8 shows this for an

observing frequency of 327 MHz. The best time resolution incoherent dedispersion offers at this frequency is about 30 μs, at the very lowest DMs. At a DM of ~ 100, the best achievable time resolution rises to ~ 100 μs. Detailed study of pulse profiles often requires sub-microsecond time resolution, especially for fast pulsars, which is just not possible to obtain using incoherent dedispersion at these frequencies (the situation is much better at higher observing frequencies of a few GHz). Moreover the scatter broadening of the pulse, a steeply rising function of DM (eq. 15), begins to dominate above a DM of ~ 100, imposing severe restrictions on achievable time resolution. This problem, too, is less severe at higher frequencies. To study pulsars with large dispersion measure and scatter broadening in the inner regions of the galaxy, it is therefore best to observe at GHz frequencies, although the expected flux from pulsars at these frequencies is much lower because of their steep spectra.

5.2. COHERENT DEDISPERSION

Hankins (1971) developed a method of removing the dispersion in pulsar signal without the need of splitting the band into narrow pieces, and hence overcoming the limitation on time resolution discussed above. This process corrects for the dispersion delay *before* the signal is passed through a detector, and hence carries the name *coherent dedispersion*. To understand how this process works, let us look at the propagation phase factor $\phi_{\rm p}$ introduced in eq. 10. Taylor expanding the phase around the lower edge of the RF band, $\nu_{\rm l}$, one obtains

$$\phi_{\rm p} = \phi_{\rm p0} + \phi'_{\rm p}(\nu_{\rm l})\,(\nu - \nu_{\rm l}) + \phi''_{\rm p}(\nu_{\rm l})\frac{(\nu-\nu_{\rm l})^2}{2!} + \cdots$$

where prime denotes differentiation with respect to ν, thus

$$\begin{aligned} \phi_{\rm p0} \;=\; \phi_{\rm p}(\nu_{\rm l}) \;&=\; 2\pi\nu_{\rm l}\frac{L}{c}\left(1 - \frac{\nu_{\rm p}^2}{2\nu_{\rm l}^2}\right) \\ \phi'_{\rm p}(\nu_{\rm l}) \;&=\; 2\pi\frac{L}{c}\left(1 + \frac{\nu_{\rm p}^2}{2\nu_{\rm l}^2}\right) \end{aligned}$$

and so on.

Noting that $\nu - \nu_{\rm l}$ is the baseband frequency $\nu_{\rm b}$, and that $\phi'_{\rm p}(\nu_{\rm l})$ is the net propagation delay $\tau_{\rm l}$ at the lower edge of the RF band, we can rewrite $\phi_{\rm p}$ as

$$\phi_{\rm p} = \phi_{\rm p0} + 2\pi\nu_{\rm b}\tau_{\rm l} + 2\pi\nu_{\rm b}\sum_{k=2}^{\infty}\phi_{\rm p}^{(k)}\frac{\nu_{\rm b}^{k-1}}{2\pi(k!)} \qquad (16)$$

where

$$\phi_{\rm p}^{(k)} \equiv \left[\frac{d^k \phi_{\rm p}}{d\nu^k}\right]_{\nu=\nu_{\rm l}}$$

In eq. (16) the first term is a constant phase factor through the band, and does not affect the signal since the origin of the phase is arbitrary anyway. The second term corresponds to a linear phase gradient through the band, which amounts to an overall shift of time origin for the whole band. The process of incoherent dedispersion makes use of this term: by splitting the signal into several sub-bands (of different $\nu_{\rm l}$) and correcting for the difference in this term between the sub-bands. The third term, which is the sum of all higher order terms in the Taylor expansion, represents the *differential* delay between the frequencies within the band. In the incoherent dedispersion process this term remains uncorrected for within each sub-band.

The process of coherent dedispersion attempts to correct the phase of the received signal before detection, to remove the third term in eq. (16). No band-splitting is done, so the second term, which contributes one overall shift of the time origin, does not contribute to dispersion within the band. The entire in-band dispersion is contained in the third term, which we shall call the Dispersion Phase Factor $\phi_{\rm D}$. It can be easily seen by successive differentiation of $\phi_{\rm p}$ with respect to ν and evaluating the results at $\nu = \nu_{\rm l}$ that

$$\phi_{\rm p}^{(k)} = (-1)^{k-1} \cdot 2\pi \cdot \left[\frac{L}{c}\frac{\nu_{\rm p}^2}{2\nu_{\rm l}^2}\right] \cdot \frac{k!}{\nu_{\rm l}^{k-1}}$$

The term in square brackets is easily identified: it is the Dispersion Delay $\mathcal{D}_\nu$ (cf. eq. 11) at $\nu = \nu_{\rm l}$. We shall denote this term as $\mathcal{D}_{\rm l}$. The Dispersion Phase Factor can now be written as

$$\begin{aligned}
\phi_{\rm D} &= 2\pi\nu_{\rm b} \sum_{k=2}^{\infty} (-1)^{k-1} \cdot \mathcal{D}_{\rm l} \cdot 2\pi \cdot \frac{k!}{\nu_{\rm l}^{k-1}} \cdot \frac{\nu_{\rm b}^{k-1}}{2\pi(k!)} \\
&= 2\pi\nu_{\rm b} \sum_{k=2}^{\infty} (-1)^{k-1} \cdot \mathcal{D}_{\rm l} \cdot \left(\frac{\nu_{\rm b}}{\nu_{\rm l}}\right)^{k-1} \\
&= 2\pi\nu_{\rm b}\mathcal{D}_{\rm l} \sum_{m=1}^{\infty} \left(-\frac{\nu_{\rm b}}{\nu_{\rm l}}\right)^{m}
\end{aligned}$$

This is a geometric series that sums to

$$\phi_{\rm D} = -2\pi\nu_{\rm b}\mathcal{D}_{\rm l}\left[\frac{\nu_{\rm b}/\nu_{\rm l}}{1+\nu_{\rm b}/\nu_{\rm l}}\right] \qquad (17)$$

as long as $\nu_{\rm b} < \nu_{\rm l}$ over the whole band, or in other words, the bandwidth BW is smaller than the frequency at the lower edge of the RF band (which is usually the case in radio observations).

The steps involved in coherent dedispersion are now clear:

- Obtain a time series by sampling the baseband voltage $V(t)$ at the Nyquist rate (sample rate = 2×the bandwidth).
- Fourier transform the time series to the frequency ($\nu_{\rm b}$) domain. This yields
$$A(\nu_{\rm b}) \cdot {\rm e}^{-i2\pi\nu_{\rm b}(t-\tau_{\rm l})} \cdot {\rm e}^{i\phi_{\rm p0}} \cdot {\rm e}^{i\phi_{\rm D}}$$
- Multiply the above spectrum by ${\rm e}^{-i\phi_{\rm D}}$, to obtain
$$A(\nu_{\rm b}) \cdot {\rm e}^{-i2\pi\nu_{\rm b}(t-\tau_{\rm l})} \cdot {\rm e}^{i\phi_{\rm p0}}$$
- Inverse Fourier transform back to time domain to obtain the corrected voltage time series $V_c(t)$. This is now free of in-band dispersion. This voltage can now be passed through a detector, preserving the time resolution offered by the full bandwidth.

In practice, one would split the time series of baseband voltage into sections of a convenient length for carrying out Fourier transforms. In doing so, one must keep in mind that the coherent dedispersion procedure is akin to convolution, and therefore the result of every section should depend also on its neighbouring sections. A proper book-keeping of these edge effects is mandatory.

Undoubtedly this is the best technique for dispersion correction. However its use has been limited till recently due to the prohibitive requirement of computing power. Dedicated processors had been built for the purpose, which usually catered to limited bandwidths, restricting their use to high time-resolution studies of a few very bright pulsars. But in the last five years or so the world has seen an explosion in affordable computing power, as well as the availability of high-speed data recording systems. This has resulted in coherent dedispersion being used much more widely than before. This technique has already made very significant contributions towards high-precision pulsar timing. If this trend continues, then coherent dedispersion may soon be regarded as the standard technique for dispersion removal.

6. Pulsar Survey Procedure

A pulsar survey is essentially an exercise in finding signals of unknown period and dispersion measure from unknown directions in the sky. To reach the desired levels of sensitivity, usually long integrations (several minutes) per beam position are necessary even with the most powerful radio telescopes. On the other hand, to detect fast-spinning pulsars such as millisecond pulsars, one must have sub-millisecond sampling and recording of the

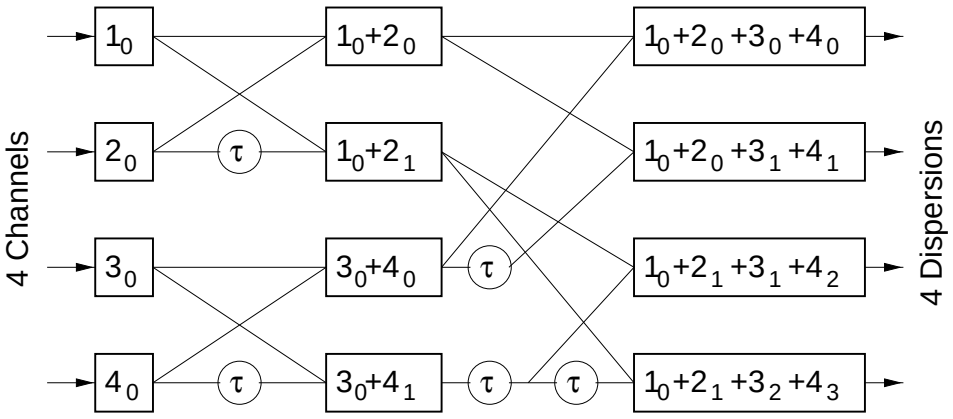

Figure 9. The tree algorithm of dedispersion, displayed here for 4 frequency channels. At the output are 4 dedispersed time series, with delays going from 0 to 3τ across the band. The numbers correspond to frequency channel identities, and the subscripts the delays, in units of τ, applied to the time series of the numbered channels. The method is easily extended to any 2^n channels. After Taylor (1974).

data. These two requirements result in very long data streams taken at a beam position in the sky, repeated for all the beam positions covering the survey area. The best technique to look for periodicity in such long data streams is Fourier analysis: the pulsed signal would show up as enhanced Fourier amplitudes at the pulse frequency (reciprocal of the pulse period) and its harmonics. One problem is that the pulse broadening due to dispersion and scattering would considerably reduce the strength of the pulsed signal. While the latter cannot be helped, it is necessary to remove the effects of dispersion to the extent possible to improve the detectability of a pulsar.

Since one does not know the dispersion measure of the pulsar to start with, the data for every field has to be dedispersed for a large number of trial DMs. One usually adopts the incoherent dedispersion technique for this procedure, as this is less demanding on computing power. As explained above, at each beam position the observing band is split into a number of frequency channels and the signal from each channel is detected, integrated for a pre-set "sampling" time (usually of order a few hundred microseconds); then sampled and recorded at the rate of one data sample per sampling time per channel. The recording is continued for the desired integration time at the beam position. This is repeated at all beam positions.

The first step of the analysis begins with the generation of dedispersed time series for a number of trial DMs. A convenient method for this is the tree algorithm developed by Taylor (1974), illustrated in figure 9. This process starts with a 2^n frequency channel data sequence and outputs dedis-

persed time series for 2^n different DMs, corresponding to total dispersion delay over the band of $0,\ \tau,\ 2\tau, \ldots, (2^n - 1)\tau$. The fixed delay unit τ is usually chosen to be the sampling interval. The advantage of this method is that only n, rather than 2^n additions per output sample is required in each dedispersed sequence, but the disadvantage is the assumption of a linear delay gradient across the band. For very wide bands used nowadays to gain sensitivity, non-linearities are significant, and this is a handicap. Various techniques, including splitting the large band into small sub-bands, applying tree algorithm within each but using non-linear corrections across them, as well as 'stretching' the original band to make the effective dispersion slope linear, have been used to overcome this limitation.

The next step consists of doing a Fourier transform of the dedispersed time series to obtain a *fluctuation spectrum*. Standard fast Fourier transform (FFT) techniques, optimized to handle real rather than complex input (since there are no imaginary parts of the time series), are used. Mixed-Radix algorithms often yield better performance than the basic Radix-2 FFT.

After the FFT comes the step of *Harmonic Folding*. Depending on the width of the pulse, the signal of a pulsar is distributed into a number of harmonics in the Fourier domain. Harmonic folding attempts to put these signals together to improve the signal-to-noise ratio and hence detectability of the periodic signal. This amounts to a search in the *duty-cycle space*. Harmonic folding is conducted in two phases: first, the *incoherent* harmonic folding using the Fourier amplitudes alone, and then the *coherent* folding using both amplitudes and phases of Fourier components.

The process of incoherent harmonic folding is illustrated in figure 10. The original power spectrum of the dedispersed time sequence is expanded by a factor of 2 in frequency and added to the original spectrum, thus adding the power at every frequency to that at twice the frequency. This replaces the original power spectrum and the process is repeated n times to add up the powers in harmonic numbers 2^k, $k = 1, \ldots, n$. A similar technique can be employed to also add up powers at harmonic numbers 3^k, 5^k etc. Now it is not necessary that the signal-to-noise ratio of a pulsar, even if present, should continue to improve as harmonic folding progresses: the harmonics beyond a point may just be too weak to add any appreciable signal. From then on, further folding will add noise to the existing harmonics and worsen the signal-to-noise ratio. Therefore at every stage of the incoherent harmonic fold, the frequencies with top-ranked signal-to-noise ratios are saved for further processing. Some redundancy check is also done at this stage: harmonically related candidates are referred back to their fundamentals to the extent possible.

The coherent harmonic fold operates on the frequencies chosen by the

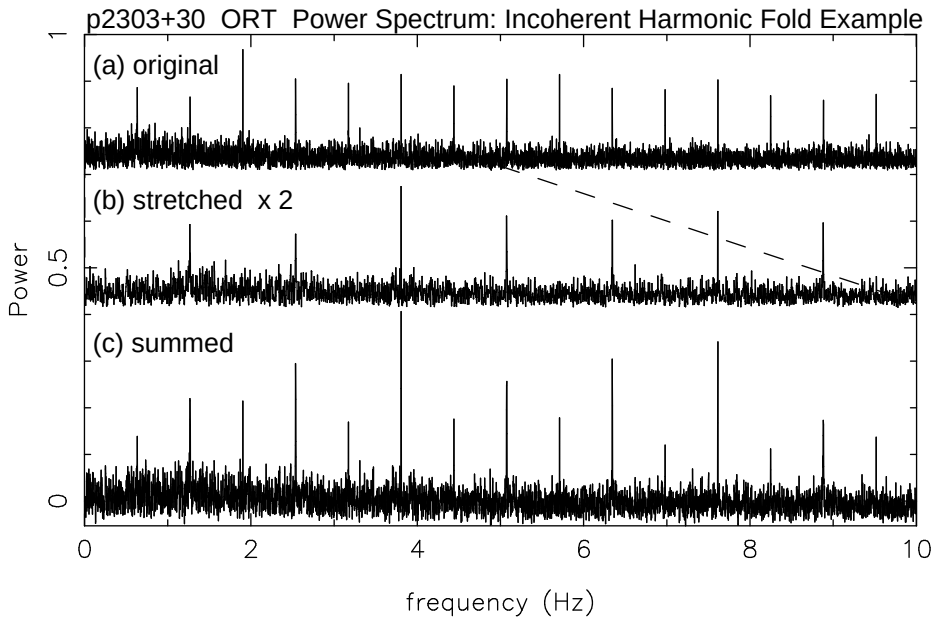

Figure 10. Example of incoherent harmonic folding on the fluctuation spectrum of the known pulsar PSR 2303+30. Panel (a) shows the original power spectrum (only a portion of the spectrum–from 0 to 10 Hz–is displayed) of the dedispersed data stream. Panel (b) shows the same spectrum after stretching by a factor of two in frequency. Panel (c) shows the sum of (a) and (b), and is the result of first stage of incoherent harmonic folding. Power at all frequencies have now been added to their first harmonics, resulting in an improvement in the signal-to-noise ratio of the even harmonics of the pulsar in the spectrum. This process is repeated several times on the summed spectra to add up harmonic numbers 2,4,8,16... etc. At each stage of the folding the top candidates above a certain threshold are shortlisted and saved.

incoherent folding. It collects from the original spectrum the full complex amplitudes at each chosen frequency and its harmonics, and Fourier transforms this series back to time domain to obtain a coarsely sampled pulse profile. The signal-to-noise ratio of this profile is estimated. This is repeated for all the chosen frequencies. If a chosen frequency (or any of its harmonics) happen not to be coincident with the centre of a spectral bin, then to obtain the complex amplitude at the desired frequency a summation is performed over complex amplitudes at several neighbouring spectral bins with, usually, $sin(x\pi)/x\pi$ amplitude weighting, and a phase rotation of $x\pi$, where x is the distance in units of bin width between the desired frequency and the neighbouring bin-centred frequencies.

If the signal-to-noise ratio in the pulse profiles obtained this way exceeds a pre-set threshold, the frequency is listed as a possible pulsar candidate. After this, a visual examination is usually made of these candidates and

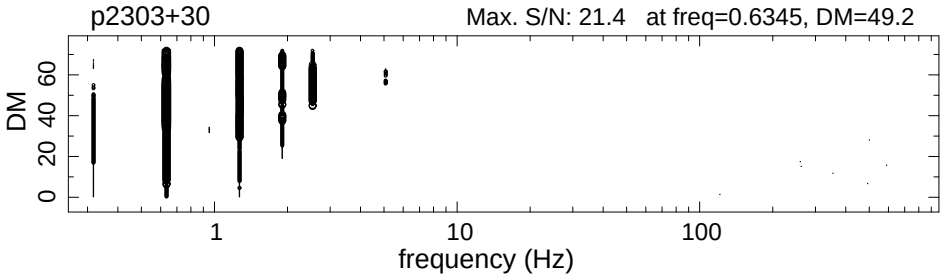

Figure 11. Candidates picked using survey procedure from a beam position containing PSR 2303+30 at the Ooty Radio Telescope. The abscissa is the (logarithm of) the pulse frequency and the ordinate is the dispersion measure. The size of the symbol is signal-to-noise-ratio (S/N) coded: larger symbols correspond to larger S/N after coherent harmonic folding. Candidates at the pulse frequency of 0.6345 Hz, as well as at 2,3,4,8 and 0.5 times the pulse frequency have been picked: they survive through the redundancy check applied because the frequencies are very slightly different from being exact multiples, as is usually the case if the true pulse frequency is not bin-centred. Candidates with similar frequencies are picked at several neighbouring DMs, which is one of the standard characteristics of a true pulsar rather than an isolated noise peak. This pulsar is so strong that at the fundamental frequency as well as at first harmonic it has been picked at all DMs-from 0 to 70, albeit with varying S/N. The true Dispersion Measure of the pulsar is 49.9.

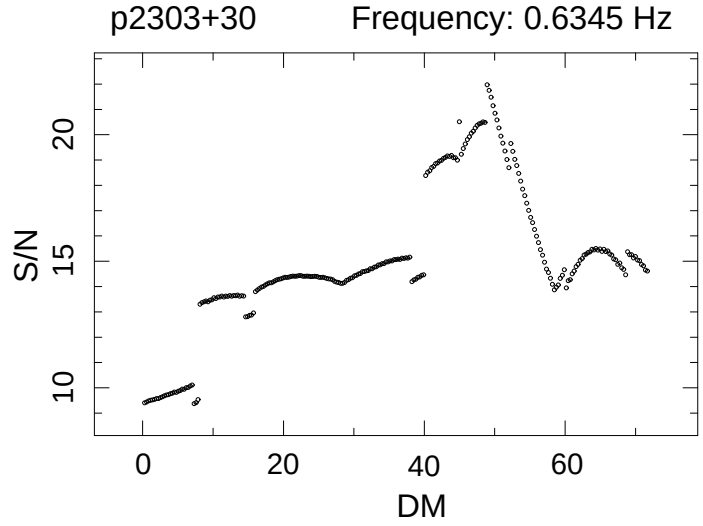

Figure 12. The signal-to-noise ratio after coherent harmonic folding versus dispersion measure for the fundamental frequency of PSR 2303+30, as picked in the previous figure. A number of frequencies, differing very slightly, around the true pulse frequency are picked by the procedure. Of them, the one with the highest S/N for a given DM is chosen for plotting. The same frequency may not have the highest S/N in all DMs–the change in the dominating frequency is reflected in discontinuous jumps in S/N in this figure. The maximum S/N occurs close to the true DM of 49.9.

shortlists are prepared. The promising candidates undergo time-domain folding with periods and DMs chosen over a range around the values obtained from the survey. This serves to further refine the parameters of the candidate. For confirmation, these fields are usually re-observed. Some characteristics of candidates picked from a field containing a known pulsar are shown in figures 11 and 12. These procedures vary somewhat between groups, for a description of the methods adopted in the recently concluded Parkes survey see Lorimer (1994), and Camilo (1995) discusses the strategy adopted in the Princeton-Arecibo surveys.

An important aspect of pulsar survey is learning to deal with interference: there are locally generated signals which can display characteristics very similar to pulsars. These interfering frequencies (which include the mains frequency and its harmonics) are usually catalogued and removed at an early stage of the analysis of each field, but also other site-specific solutions may become necessary in some cases.

As must be clear to the reader, because of the very large number of repetitive operations involved, the data analysis for a pulsar survey is an extremely computation-intensive procedure. Improvements in the computer industry is driving this field too: sensitive pulsar surveys for very short period pulsars, which would have been extremely difficult some years ago, are now being undertaken by several groups around the world. Nonetheless, the procedure described above remains poorly sensitive to pulsars in short-period binary systems, as the apparent frequency of such pulsars can change significantly during the integration time because of Doppler effect. Looking for these pulsars adds an extra dimension to the search, that of *acceleration* in the orbit. Acceleration search has been used profitably in targeted surveys towards Globular clusters, where only a very small area of the sky is surveyed, and the dispersion measure is also known within a small margin. Doing acceleration search routinely in general, all-sky surveys is still somewhat out of reach of present computing resources. But even this hurdle may become surmountable in the near future, either by speeding up computers or by building radio telescopes with very large collecting area (for example, the square-kilometre arrays proposed by various nations) which will cut down the integration time needed per field, and will thus be less susceptible to frequency drifts by acceleration. One looks forward to exciting new discoveries in this relatively unexplored area of highly accelerated pulsars.

Acknowledgements

It is a pleasure to acknowledge years of discussion and collaboration with my colleagues in the pulsar group at the Raman Research Institute and the

National Centre for Radio Astrophysics, Pune, particularly with Avinash Deshpande and Yashwant Gupta. In addition, R. Ramachandran, Sanjay Upreti, Dipanjan Mitra and Lakshmy P Usha have been involved in various stages of software development and data collection over the years. Many people, including P. S. Ramkumar, T. Prabu, G. Markandeyulu, M. Girimaji, A. Deshpande, Y. Gupta, J. G. Ables and D. McConnel have contributed to the hardware used for pulsar observations at the Ooty Radio Telescope. I would like to thank NATO for financial assistance to attend this interesting Advanced Study Institute.

References

1. Bhattacharya, D., Wijers, R. A. M. J., Hartman, J., Verbunt, F. 1992, *Astr. Astrophys.*, **254**, 198
2. Camilo, F. 1995, Ph. D. Thesis, Princeton University
3. Deshpande, A. A. 1989, *Technical Report on Pulsar Receiver for the GMRT*, Raman Research Institute
4. Hankins, T. H. 1971, *Astrophys. J.*, **169**, 487
5. Hankins, T. H., Rickett, B. J. 1975, In *Methods in Computational Physics*, eds. B. Adler, S. Fernback, M. Rotenberg, Academic Press, **14**, p. 55
6. Lorimer, D. 1994, Ph. D. Thesis, University of Manchester
7. Ramachandran, R., Mitra, D., Deshpande, A. A., McConnel, D., Ables, J. G., 1997, preprint
8. Rickett, B. J. 1977, *Ann. Rev. Astr. Astrophys.*, **15**, 479
9. Rickett, B. J. 1990, *Ann. Rev. Astr. Astrophys.*, **28**, 561
10. Taylor, J. H. 1974, *Astr. Astrophys. Suppl.*, **15**, 367
11. Taylor, J. H., Cordes, J. M. 1993, *Astrophys. J.*, **411**, 674
12. Vivekanand, M., Narayan, R., Radhakrishnan, V. 1982, *J. Astrophys. Astr.*, **3**, 237